HHS Public Access

Author manuscript

J Mech Behav Biomed Mater. Author manuscript; available in PMC 2020 September 01.

Published in final edited form as:

J Mech Behav Biomed Mater. 2019 September ; 97: 65–73. doi:10.1016/j.jmbbm.2019.05.001.

Reliable Preparation of Agarose Phantoms for Use in Quantitative Magnetic Resonance Elastography

Grace McIlvain[1], **Elahe Ganji**[2], **Catherine Cooper**[3], **Megan L Killian**[1], **Babatunde A Ogunnaike**[4], **Curtis L Johnson**[1]

[1]Department of Biomedical Engineering, University of Delaware; Newark, DE

[2]Department of Mechanical Engineering, University of Delaware; Newark, DE

[3]Department of Linguistics and Cognitive Science, University of Delaware; Newark, DE

[4]Department of Chemical and Biomolecular Engineering, University of Delaware; Newark, DE

Abstract

Agarose phantoms are one type of phantom commonly used in developing *in vivo* brain magnetic resonance elastography (MRE) sequences because they are inexpensive and easy to work with, store, and dispose of; however, protocols for creating agarose phantoms are non-standardized and often result in inconsistent phantoms with significant variability in mechanical properties. Many magnetic resonance imaging (MRI) and ultrasound studies use phantoms, but often these phantoms are not tailored for desired mechanical properties and as such are too stiff or not mechanically consistent enough to be used in MRE. In this work, we conducted a systematic study of agarose phantom creation parameters to identify those factors that are most conducive to producing mechanically consistent agarose phantoms for MRE research. We found that cooling rate and liquid temperature affected phantom homogeneity. Phantom stiffness is affected by agar concentration (quadratically), by final liquid temperature and salt content in phantoms, and by the interaction of these two metrics each with stir rate. We captured and quantified the implied relationships with a regression model that can be used to estimate stiffness of resulting phantoms. Additionally, we characterized repeatability, stability over time, impact on MR signal parameters, and differences in agar gel microstructure. This protocol and regression model should prove beneficial in future MRE development studies that use phantoms to determine stiffness measurement accuracy.

Keywords

Magnetic Resonance Elastography; Phantoms; Agarose; Stiffness; Viscoelasticity

Corresponding Author: Curtis L Johnson, PhD, 150 Academy St, Newark, DE 19716, clj@udel.edu.

1. Introduction

Magnetic resonance elastography (MRE) is an imaging technique used to measure viscoelastic mechanical properties of soft tissue *in vivo* (Muthupillai et al., 1995). MRE captures mechanical deformations induced by harmonic vibration through phase-contrast magnetic resonance imaging (MRI) to determine viscoelastic properties such as shear modulus, stiffness, and damping ratio. These properties reflect the microstructural health of tissues such as the brain (Sack et al., 2013); for example, MRE studies have shown brain stiffness to decrease with the presence and progression of neurodegenerative diseases such as multiple sclerosis (Streitberger et al., 2012; Wuerfel et al., 2010) and Alzheimer's disease (Murphy et al., 2016, 2011). Mechanical properties of the healthy brain determined from MRE have been shown to differ in older adults (Arani et al., 2015; Hiscox et al., 2018) and in children (McIlvain et al., 2018), and reflect cognitive function (Johnson et al., 2018; Schwarb et al., 2016). Advances in brain MRE measurement accuracy and precision come from the development of novel mechanical actuators, pulse sequences, and inversion algorithms, which have facilitated high-resolution, whole-brain mapping of mechanical properties (Braun et al., 2014; Johnson et al., 2016; Murphy et al., 2018).

Quantifying the accuracy and precision of *in vivo* measurements remains a key challenge to the development of novel MRE methodology. Consequently, phantoms are frequently used during technical development to evaluate new techniques on objects with known properties. However, while phantoms serve a critical role in MRE technology development, researchers often have to choose between phantoms that provide standardized mechanical properties or phantoms that provide desirable MR signal parameters. The former can be expensive and difficult to customize, while the latter require additional characterization of expected mechanical properties, which can vary between phantoms due to inconsistent preparation. Creating accurate, consistent phantoms for use in sequence development and data collection will facilitate advances in MRE technology.

Phantoms with standardized mechanical property contrast have been used in acoustic radiation force impulse imaging (Duan et al., 2014), optical coherence tomography (Lamouche et al., 2012), and, most frequently, in ultrasound (Cafarelli et al., 2017) and ultrasound elastography (Li et al., 2011; Troia, Cuccaro, & Schiavi, 2017). The CIRS 049 and 49a are the gold standard phantoms for use in ultrasound (Cournane et al., 2012), but many others are also available. The CIRS 049 ultrasound phantom has been used in previous MRE studies (Baghani et al., 2011; Barnhill et al., 2017; Honarvar et al., 2013), however these phantoms include very stiff inclusions up to 80 kPa (CIRS, 2008) that do not reflect the typical properties and contrast in the brain where shear stiffness is typically on the order of 1-5 kPa depending on measurement technique (Budday et al., 2017; Chatelin et al., 2010). When measured with MRE at 50 Hz vibration, healthy brain viscoelastic shear stiffness is typically between 2.5 and 4 kPa (Hiscox et al., 2016), with stiffness of some meningioma tumors reported up to 8 kPa (Hughes et al., 2015; Murphy et al., 2013), thus the very high stiffness of the CIRS 049 inclusions is not reflective of the human brain. Additionally, these ultrasound phantoms were not designed for MRI and do not have optimal MR signal parameters – proton density or T_1- and T_2-relaxation times – that ultimately decrease the signal-to-noise ratio of the resulting images. The non-optimal stiffnesses and MR signal

parameters in these phantoms require tailored imaging and inversion approaches to recover mechanical properties accurately, such as higher vibration frequency, thus making them less useful as a model for brain MRE.

Phantoms with suitable MR signal parameters are often created from a variety of different materials and are tailored to suit different applications. Silicone-based materials have been used in MRE and provide tunable properties with long shelf-life (Brinker and Klatt, 2016; Brinker et al., 2018; Kashif et al., 2013; Leclerc et al., 2012; Lefebvre et al., 2016; Plewes et al., 2000; Solamen et al., 2018; Yasar et al., 2013), but creating phantoms with inclusions of varying geometry can be challenging with these materials. Agarose is one common phantom material used in MRE because it is relatively inexpensive, and phantoms can easily be created in different sizes and shapes, while old phantoms are easily disposed of (Normand, Lootens, Amici, Plucknett, & Aymard, 2000). Furthermore, agar is a plant-based substance that forms a gel when mixed with water and heated, and the water-based nature of the gel results in phantoms with excellent MR signal characteristics.

Agarose phantoms have been used in many different MRE studies (Johnson et al., 2013; Le et al., 2006; Solamen et al., 2018) because their mechanical properties are easily tailored via agar concentration (Normand et al., 2000). However, the properties of these phantoms are often subject to random variability as a result of inconsistencies in several parameters controlled during phantom creation (Solamen et al., 2018), which may influence the chemical makeup of the material. For example, oxidation of agarose to carboxylated agarose has been shown to affect gel properties (Forget, Pique, Ahmadi, Lüdeke, & Shastri, 2015 Rüther et al., 2017), a reaction that may vary based on how the phantom is created. In this study, we aim to determine (and quantify) how agar phantom creation affects their mechanical properties to enable the development of a protocol for reliable, consistent, and stable agarose phantom preparation for MRE.

2. Methods

The desired outcome of this study is the creation of a replicable, homogenous, and mechanically accurate agarose phantom to be used as a model of the brain in MRE studies. To achieve this, we varied several phantom creation parameters systematically according to a statistical design of experiment, to determine (and quantify) the effect of each on the resulting mechanical properties measured with MRE (see below). All phantoms were created in a controlled environment by the same experimenter to reduce variability. Within 36 hours of creation, each phantom was brought to room temperature and imaged on a Siemens 3T Prisma MRI scanner (Erlangen, Germany).

2.1 Imaging Protocol

MRE displacement data were acquired using a single-shot echo-planar imaging (EPI) sequence. The resulting MRE images had $2.0 \times 2.0 \times 2.0$ mm^3 isotropic spatial resolution and encoded displacements from 50 Hz vibrations delivered to the phantom via Resoundant pneumatic actuator system with passive driver (Rochester, MN). Additional standard imaging parameters included: field-of-view = 240×240 mm^2; matrix = 120×120; 72 total

slices; TR/TE = 10080/78 ms. Total MRE acquisition time was approximately 5 minutes for each phantom. Phantoms were brought to room temperature prior to scanning.

The nonlinear inversion algorithm (NLI) was used to calculate phantom viscoelastic properties from MRE displacement data (McGarry et al., 2012; Van Houten et al., 2001). NLI is a finite element-based inversion algorithm that iteratively solves for the spatial distribution of mechanical properties in the object. The outputs from NLI are maps of the complex viscoelastic shear modulus, G = G' + iG", where G' is the storage modulus and G" is the loss modulus. From these parameters we calculate shear stiffness, $\mu = 2|G|^2/(G'+|G|)$ (Manduca et al., 2001), and damping ratio, $\xi = G''/2G'$ (McGarry and Van Houten, 2008). NLI has been shown to produce accurate measurements of shear modulus in phantoms compared to traditional dynamic mechanical shear testing (Solamen et al., 2018).

Figure 1 shows an overview of the phantom MRE experiment: example MRI magnitude image, full vector displacement fields, and calculated stiffness map from NLI. The primary outcome of interest in the experiments was phantom shear stiffness; however, damping ratio, storage modulus, and loss modulus are additionally reported in Supplemental Information.

2.2 Phantom Creation Protocol

Phantoms were made from Sigma-Aldrich 9799 plant agar (St. Louis, MO) that was mixed with water and salt, heated on a Corning PC-420D hotplate (Corning, NY) until the liquid reached the target temperature, and then cooled to form a solid gel. Temperature was measured periodically during the heating process using a standard scientific thermometer; as a result of constant stirring of the liquid, temperature was assumed to be homogenous throughout. Phantom creation parameters of interest included agar concentration, salt concentration, hot plate temperature, stir rate, final liquid temperature, whether a lid was used during heating, and cooling rate determined by cooling location. Each phantom was created with 1000 mL of water except for those created without a lid, which were created with 1100 mL to account for water loss from evaporation. Each phantom was solidified and housed in a disposable plastic square container (size: 6-1/8" × 6-1/8" × 3-3/8"; 1180 mL volume). Each container held one phantom and phantoms were housed and scanned in the container where they solidified.

2.3 Impact of Phantom Creation Parameters on Stiffness

We aimed to determine phantom creation parameters that affect resulting mechanical properties, or which result in undesirable phantom characteristics, such as spatially inhomogeneous properties. A two-level, six-factor, resolution IV fractional factorial screening design implemented with JMP Pro 13.1.0 (SAS Institute, Inc.; Cary, NC) was chosen to determine, efficiently, which parameters and which parameter interactions significantly affect mechanical properties. This experimental design was chosen for its efficiency; being a Resolution IV design allows estimation of all possible two-way interaction effects without confounding them with any other significant effects. The experiments involved investigating the phantom creation process at prescribed combinations of the following high and low values for each of six parameters: hot plate temperature (300 °C v. 550 °C), salt content (0.3%wt. v. 0.9%wt.), stir rate (100 rpm v. 800 rpm),

presence of a lid during heating (yes v. no), final liquid temperature (84 °C v. 96 °C), and the cooling location (room temperature, refrigerator, ice bath) – indicative of cooling rate. Aluminum foil was used to cover the beaker tightly for trials with a lid during heating. Agar concentration (1.0%wt.) was held constant for all phantoms in this screening experiment. Total heating time for creating each phantom was recorded. We avoided cooling two phantoms in the refrigerator simultaneously so that each phantom was cooled consistently. Consequently, we monitored the refrigerator temperature to ensure that it remained below 46 °C during cooling of each phantom.

Following imaging, we visually examined MRI magnitude and stiffness images for gel heterogeneity, marking such phantoms as failures. These heterogeneities occurred in a similar manner in each failed phantom and are easily recognized visually as large areas of inconsistent stiffness and magnitude in the center-bottom of the phantom. After excluding data associated with undesirable patterns of gelling in phantoms, we used the JMP Fit Model tool to analyze the remaining data, determining the statistically significant main and interaction effects of each tested parameter on mechanical properties. We followed this screening study with a response surface design to investigate mechanical properties of phantoms created at high, middle, and low values of the phantom creation parameters determined to be significant. Such a design would allow us to develop a higher order (possibly nonlinear) mathematical relationship between the significant parameters and the mechanical properties of the resulting phantoms. New phantoms were created from combinations of the significant parameters at the three levels, leaving other non-significant parameters held constant. The resulting data were analyzed using multivariate nonlinear regression to create a model relating phantom stiffness to creation parameters.

2.4 Impact of Agar Concentration on Phantom Stiffness

To measure the effect of agar concentration in our experimental as a parameter in our model, we created phantoms with varying agar concentration with other parameters held constant. Four replicates of phantoms with 0.6, 0.8, 1.0, and 1.2%wt agar concentrations were created and imaged. Other parameters were held at intermediate values based on the results of the previous experiment: 450 °C hot plate temperature, 0.5%wt salt concentration, 600 rpm stir rate, lid present, 90 °C final liquid temperature, and phantoms cooled in the refrigerator. We fit the dependence of phantom stiffness on agar concentration using a quadratic model. We measured the impact of agar concentration separately from the other parameters because it was already known to have affect stiffness (Normand et al., 2000).

2.5 T_1- and T_2-relaxation Times

We measured the T_1- and T_2-relaxation times for agar phantoms for each agar concentration (0.6, 0.8, 1.0, 1.2%wt.). T1-relaxation maps were acquired for the four phantoms at each concentration with the following imaging parameters: 1.9 × 1.9 × 2.0 mm^3 resolution; field-of-view = 240 × 240 mm^2; matrix = 128 × 128; 48 total slices; TR/TE = 15.0/1.78 ms; and four flip angles at 5°, 12°, 19°, and 26°. T_2-relaxation maps were acquired in the same phantoms over the same imaging volume using a multi-echo sequence with parameters TR = 7500 ms and twelve evenly spaced TEs from 12.5 to 150 ms. Maps were spatially averaged

and mean values and standard deviations were calculated across all four samples for each concentration.

2.6 Phantom Stiffness Repeatability and Long-Term Stability

To test repeatability of the phantom creation protocol, ten replicate phantoms were created using intermediate creation parameters based on our fractional factorial experiment results: 1.0%wt. agar concentration, 450 °C hot plate temperature, 0.5%wt. salt concentration, 600 rpm stir rate, lid present, 90 °C final liquid temperature, and samples cooled in the refrigerator. MRE was performed on each phantom and repeatability of stiffness was determined via the coefficient of variation (CV) – the ratio of standard deviation to the mean – across all ten phantoms. Four of these phantoms were scanned three times to estimate measurement variability. We characterized the stability of the mechanical properties in three of these phantoms over a period of five weeks. Phantoms were stored in the refrigerator during this process except for imaging, which occurred once per week over the five-week period.

2.7 Microscopy of Agar Phantom Microstructure

To explore the dependency of phantom mechanical properties on preparation protocol, we also examined the phantom microstructure. We performed microscopy on samples prepared considering the three factors which significantly affect stiffness: temperature, salt concentration, and agar concentration. Our baseline agar preparation protocol (90 °C temperature, 0.6%wt. salt, and 1.0%wt. agarose) was used, along with samples having a high and a low value for each of the three factors of interest: temperature (84 °C and 96 °C), salt concentration (0.3%wt. and 0.9%wt. salt), and agar concentration (0.6%wt. and 1.4%wt.). After curing in a cryomold, Tissue-Tek OCT medium (Sakura Finetek; Torrance, CA) was used for cryo-preparation. Samples were kept in −80°C and cryosectioned at 200 μm thickness (−27 to −30 °C). Sections were imaged two hours after sectioning using an upright microscope at 5x magnification.

3. Results

3.1 Impact of Phantom Creation Parameters on Stiffness

Table 1 shows magnitude of the effect of individual parameters on phantom stiffness, and associated p-values. Of the parameters tested, only final liquid temperature and salt content significantly affected phantom stiffness at the significance level $\alpha = 0.01$ (since $p < 0.01$ in each case). A complete table of the magnitude of the effect of each parameter on G', G", μ, and ξ is in the Supplemental Information. We found that all phantoms with final liquid temperature of 84 °C and phantoms cooled in the ice bath had structural inhomogeneities as shown in Figure 2.

We also determined the interaction effects of the parameters on phantom stiffness. Figure 3 shows the normal and pareto plots of the effect size of factors at the 99% confidence level. In addition to the significant primary effects of salt content and final liquid temperature, we found that the interaction of salt and stir rate, and the interaction of stir rate and final liquid temperature, have statistically significant effects on phantom stiffness (at the $\alpha = 0.01$

significance level). Figure 4 shows leverage plots of residuals for salt content, final liquid temperature, stir rate, and their interactions.

After determining significant parameters to be final liquid temperature, salt content, and their respective interactions with stir rate, we conducted additional experiments to determine potential curvature in the response of stiffness to these significant parameters, keeping other (non-significant) parameters constant at their nominal values. Some additional considerations:

- No significant difference was found between phantoms cooled at room temperature or in the refrigerator; however, phantoms are stored long-term in the refrigerator; consequently, the refrigerator was chosen as the cooling location for the remainder of the phantoms.
- Hot plate temperature had no effect on measured outcomes, so hotter temperatures would be preferable to reduce total time; for the rest of this study 450 °C was chosen.
- An aluminum foil lid was used to cover the beaker while heating. While this did not significantly affect measured parameters, the use of a lid greatly reduced and stabilized heating times; consequently, the lid was used for the remaining duration of this study.

Figure 5 shows the cube plot and various combinations of two-dimensional contour plots of stiffness as a function of significant parameters.

3.2 Impact of Agar Concentration on Phantom Stiffness

Figure 6 shows the dependence of phantom stiffness, μ, on agar concentration, A, indicating a quadratic relationship determined via least squares regression as: $\mu = 12.56A^2 - 5.83A$, with an adjusted R^2 value of 0.918. We combined the effect of agar concentration with the significant phantom creation parameter effects described above to generate a regression model for the dependence of phantom stiffness on significant factors, which is given in Equation 1. This model with a small number of parameters describes the stiffness data with an adjusted R^2 value of 0.833.

$$\text{Stiffness (kPa)} = 12.56 \cdot A^2 - 5.83 \cdot A + 3.187 \cdot B + 0.5859 \cdot C + \left(-0.0298 \cdot (B - 0.582) \cdot (D - 460)\right) + \left(-0.000743 \cdot (C - 90.622) \cdot (D - 460)\right) - 54.58$$

A Agar Concentration (%wt)
B Salt Concentration (%wt)
C Final Liquid Temp (°C)
D Stir Rate (rpm)

*Model valid for temperatures above 84 °C

Equation 1: Regression equation for stiffness (kPa) as a function of all factors that significantly affect final stiffness value ($p < 0.01$). Effect of agar on stiffness was added to the model first, and additional factors that significantly affect stiffness were subsequently

included to reduce the remaining unexplained variation. Adjusted R^2 value for the regression model is 0.833.

3.3 T_1- and T_2-relaxation Times

The T_2-relaxation times, but not the T_1-relaxation times, of the phantoms created in this study were dependent on agar concentration (Figure 7; Table 2). A linear inverse relationship between agar concentration and T_2-relaxation time was observed ($p < 0.001$). No correlation was found between T_1-relaxation time and agarose concentration ($p = 0.617$). The observed T_1- and T_2-relaxation time relationships to agar concentration are in concordance with previous results (Yoshida et al., 2004)

3.4 Phantom Repeatability and Long-Term Stability

Mean stiffness of the ten replicate phantoms was 6.91 kPa with a standard deviation of 0.23 kPa, which is equivalent to a CV of 3.3%, and is indicative of variability of phantom creation. The CV of stiffness measures from repeated scans of the same phantoms was 0.6%, on average, and is indicative of variability in MRE stiffness measurements. The variability in phantom creation and MRE stiffness measurement are comparable to the variability in current *in vivo* brain MRE methods (Anderson et al., 2016; Johnson et al., 2016).

The stiffnesses of three phantoms were measured once a week for five weeks (Figure 8). Phantom stiffness was generally stable during the entire five weeks with an average variability in stiffness of 1.1% and a maximum difference from baseline of 2.7%. This variability is similar to the variability in phantom creation described above.

3.5 Microscopy of Agar Phantom Microstructure

Changes in temperature, salt, and agar concentration affected the microstructural composition of the gel phantom. Figure 9 presents microscopy images of gels at high, middle, and low values for each of these parameters, and which show distinct microstructural characteristics that change with each parameter. For instance, lower final liquid temperature changes the shape of the agarose network, and higher salt content results in a very sparse network. These different microstructures are the likely basis of the differences in phantom stiffness observed with MRE.

4. Discussion

While it is common to use agarose phantoms in MRE for sequence development and testing, achieving consistent mechanical properties in agarose phantoms is often challenging (Solamen et al., 2018). In addition to the well-known dependence of gel stiffness on agar concentration, in this study we found that controllable parameters during phantom creation, specifically final liquid temperature, salt content, and the interaction of the two with stir rate, significantly affect resulting phantom stiffness. These terms potentially affect oxidation of the agarose molecules, converting agarose into carboxylate agarose, which has been shown to change the structural composition of the molecule (Chhatbar et al., 2012; Su et al., 2013; Zarrintaj et al., 2018). Oxidation of agarose is a key determinant of the final gel mechanical properties (Forget et al., 2015; Rüther et al., 2017).

In addition to determining factors affecting gel mechanical properties, we also sought to determine factors that promote homogeneity of properties throughout the agarose phantom. We found that cooling the phantoms in the ice bath caused noticeable differences in phantom consistency, as the external edges of the phantom cooled far more rapidly than the center. Slower cooling in either the refrigerator or at room temperature resulted in more consistent phantom characteristics, with no significant effect on stiffness. A low final liquid temperature also resulted in inhomogeneous phantoms, likely due to incomplete dissolution of the agar in water, while phantoms created with higher liquid temperatures were uniform.

The macrostructural differences in mechanical property arising from the phantom creation protocol are of primary interest, though these differences are likely microstructural in origin. Microscopy results show a dependency of agar structure on such preparation parameters as temperature and salt concentration. While factors such as temperature, evaporation, and sectioning artifact might have affected the imaged agar structures, consistency in imaging protocol made microscopy a useful tool for comparative structural evaluation. Our results systematically show disruptions of agar structure at the microscale in phantoms with increased salt concentration and low final liquid temperature. These include changes in shape and density of network structure, which likely result in the observed differences in observed mechanical properties.

In addition to agar gel, additional materials that have been used as phantoms in MRE research include food grade tofu (Pattison et al., 2014; Van Houten et al., 2011), silicone (Kashif et al., 2013; Solamen et al., 2018), Ecoflex (Brinker and Klatt, 2016; Yasar et al., 2013), plastisol (Brinker et al., 2018; Leclerc et al., 2013; Lefebvre et al., 2016; Plewes et al., 2000), and Knox gelatin (Gordon-Wylie et al., 2018). These materials all have different benefits and are chosen for different purposes, though agarose remains popular for use in MRE because it is inexpensive, it provides good MRI image contrast, it has manipulatable mechanical properties, and it is very easy to create and dispose of. However, agar alone is not capable of replicating many properties of brain tissue that are of interest in MRE, including damping ratio and anisotropy. Brain tissue damping ratio is approximately 0.2 (Johnson et al., 2016), and damping ratio of the agar phantoms is an order of magnitude lower, at −0.017 to 0.032 (see Table S2). Brain white matter is also anisotropic due to the alignment of axonal fibers (Schmidt et al., 2016), and the agar gel phantoms can only provide isotropic properties. Despite these limitations, agar phantoms will continue to be useful for isotropic MRE studies and may be used with other materials to achieve additional, desirable characteristics.

Even though our main objective was to provide a complete understanding of factors affecting variability between phantoms, this study has several limitations. First, it is difficult to separate sources of observed variability in measured stiffness from preparation of phantoms or from MRE measurement uncertainty. Despite a consistent preparation protocol, there are likely factors beyond our control that may introduce unintended variability, such as differences between agar batches, but there is no reason to believe that these are greater than normal variability in any experimental study. Our model for determining stiffness from a reduced set of significant parameters may have reduced predictive power in this case. Validating this model with an independent sample of phantoms to determine and quantify

the amount of unexplained variance is slated for future work. We also chose to analyze primarily phantom stiffness as this is most commonly reported in brain MRE studies (Murphy et al., 2016; Schwarb et al., 2016), though some phantom designs may wish to control individual storage or loss moduli or damping ratio. We found significant dependence of storage modulus on final liquid temperature and dependence of loss modulus on salt content and final liquid temperature, and these can be used in similar regression models using the complete data included with this paper as Supplemental Information. Lastly, while we hypothesized that agar oxidation may be contributing to phantom variability, we did not explicitly assess oxidation in our samples. Future work will be devoted to further refining the parameter space through careful measurement and characterization of oxidation.

5. Conclusion

Agarose phantoms for the use in MRE are beneficial as a model for brain stiffness because they are inexpensive and easy to work with, however they often lack mechanical consistency. Aside from agar concentration, influential factors during phantom creation and their impact on stiffness were unknown. In this study, we assessed how various phantom creation parameters impact resulting stiffness. In addition to agar concentration, final liquid temperature and salt content in phantoms, as well as the interaction of these terms each with stir rate, have a significant, positive effect on stiffness. From this data we created a regression model incorporating the significant factors that can be used to reliably design agar phantoms for MRE research. Using our improved information, researchers can create agarose phantoms with low variability that are stable over a period of at least five weeks. Ultimately this protocol may be useful in future MRE technology development that require phantoms to determine measurement accuracy.

Supplementary Material

Refer to Web version on PubMed Central for supplementary material.

Acknowledgments

This research was partially supported by NIH/NIA (R01-AG058853), NIH/NIBIB (R01-EB027577), NIH/NIDDK (R01-DK113272), the University of Delaware Research Foundation, and the Delaware INBRE program, supported by a grant from NIH/NIGMS and the State of Delaware (P20-GM103446).

References

Anderson AT, Van Houten EEW, McGarry MDJ, Paulsen KD, Holtrop JL, Sutton BP, Georgiadis JG, Johnson CL, 2016 Observation of direction-dependent mechanical properties in the human brain with multi-excitation MR elastography. J. Mech. Behav. Biomed. Mater 59, 538–546. 10.1016/j.jmbbm.2016.03.005 [PubMed: 27032311]

Arani A, Murphy MC, Glaser KJ, Manduca A, Lake DS, Kruse SA, Jack CR, Ehman RL, Huston J, 2015 Measuring the effects of aging and sex on regional brain stiffness with MR elastography in healthy older adults. Neuroimage 111, 59–64. 10.1016/j.neuroimage.2015.02.016 [PubMed: 25698157]

Baghani A, Salcudean S, Honarvar M, Sahebjavaher RS, Rohling R, Sinkus R, 2011 Travelling wave expansion: A model fitting approach to the inverse problem of elasticity reconstruction. IEEE Trans. Med. Imaging 30, 1555–1565. 10.1109/TMI.2011.2131674 [PubMed: 21813354]

Barnhill E, Hollis L, Sack I, Braun J, Hoskins PR, Pankaj P, Brown C, van Beek EJR, Roberts N, 2017 Nonlinear multiscale regularisation in MR elastography: Towards fine feature mapping. Med. Image Anal 35, 133–145. 10.1016/j.media.2016.05.012 [PubMed: 27376240]

Braun J, Guo J, Lützkendorf R, Stadler J, Papazoglou S, Hirsch S, Sack I, Bernarding J, 2014 High-resolution mechanical imaging of the human brain by three-dimensional multifrequency magnetic resonance elastography at 7T. Neuroimage 90, 308–314. 10.1016/j.neuroimage.2013.12.032 [PubMed: 24368262]

Brinker S, Klatt D, 2016 Demonstration of concurrent tensile testing and magnetic resonance elastography. J. Mech. Behav. Biomed. Mater 63, 232–243. 10.1016/j.jmbbm.2016.06.020 [PubMed: 27429072]

Brinker ST, Kearney SP, Royston TJ, Klatt D, 2018 Simultaneous magnetic resonance and optical elastography acquisitions: Comparison of displacement images and shear modulus estimations using a single vibration source. J. Mech. Behav. Biomed. Mater 84, 135–144. 10.1016/j.jmbbm.2018.05.010 [PubMed: 29775815]

Budday S, Sommer G, Birkl C, Langkammer C, Haybaeck J, Kohnert J, Bauer M, Paulsen F, Steinmann P, Kuhl E, Holzapfel GA, 2017 Mechanical characterization of human brain tissue. Acta Biomater. 48, 319–340. 10.1016/j.actbio.2016.10.036 [PubMed: 27989920]

Cafarelli A, Verbeni A, Poliziani A, Dario P, Menciassi A, Ricotti L, 2017 Tuning acoustic and mechanical properties of materials for ultrasound phantoms and smart substrates for cell cultures. Acta Biomater. 49, 368–378. 10.1016/j.actbio.2016.11.049 [PubMed: 27884775]

Chatelin S, Andre C, Remy W, 2010 Fifty years of brain tissue mechanical testing: From in vitro to in vivo investigations. Biorheology 47, 255–276. 10.3233/BIR-2010-0576 [PubMed: 21403381]

Chhatbar MU, Godiya CB, Siddhanta AK, 2012 Functional modification of agarose : A facile synthesis of an agarose-saccharate derivative. Carbohydr. Polym 88, 1118–1123. 10.1016/j.carbpol.2012.01.086

CIRS, 2008 Elasticity QA Phantoms Models 049 & 049a [WWW Document].

Cournane S, Fagan AJ, Browne JE, 2012 Review of ultrasound elastography quality control and training test phantoms. Ultrasound 20, 16–23. 10.1258/ult.2011.011033

Forget A, Pique RA, Ahmadi V, Lüdeke S, Shastri VP, 2015 Mechanically tailored agarose hydrogels through molecular alloying with β-sheet polysaccharides. Macromol. Rapid Commun 36, 196–203. 10.1002/marc.201400353 [PubMed: 25250523]

Gordon-Wylie SW, Solamen LM, McMarry MDJ, Zeng W, Van Houten EEW, Gilbert G, Weaver JB, Paulsen KD, 2018 MR Elastography at 1 Hz of Gelatin Phantoms Using 3D or 4D Acquisition. J. Magn. Reson 296, 112–120. 10.1016/j.jmr.2018.08.012 [PubMed: 30241018]

Hiscox LV, Johnson CL, McGarry MDJ, Perrins M, Littlejohn A, van Beek EJR, Roberts N, Starr JM, 2018 High-resolution magnetic resonance elastography reveals differences in subcortical gray matter viscoelasticity between young and healthy older adults. Neurobiol. Aging 65, 158–167. 10.1016/j.neurobiolaging.2018.01.010 [PubMed: 29494862]

Hiscox LV, Johnson CL, Barnhill E, McGarry MDJ, Huston J, van Beek EJR, Starr JM, Roberts N, 2016 Magnetic resonance elastography (MRE) of the human brain: technique, findings and clinical applications. Phys. Med. Biol 61, R401–R437. 10.1088/0031-9155/61/24/R401 [PubMed: 27845941]

Honarvar M, Sahebjavaher R, Sinkus R, Rohling R, Salcudean SE, 2013 Curl-based finite element reconstruction of the shear modulus without assuming local homogeneity: Time harmonic case. IEEE Trans. Med. Imaging 32, 2189–2199. 10.1109/TMI.2013.2276060 [PubMed: 23925367]

Hughes JD, Fattahi N, Van Gompel J, Arani A, Meyer F, Lanzino G, Link MJ, Ehman R, Huston J, 2015 Higher-Resolution Magnetic Resonance Elastography in Meningiomas to Determine Intratumoral Consistency. Neurosurgery 77, 653–658. 10.1227/NEU.0000000000000892 [PubMed: 26197204]

Johnson CL, McGarry MDJ, Van Houten EEW, Weaver JB, Paulsen KD, Sutton BP, Georgiadis JG, 2013 Magnetic resonance elastography of the brain using multishot spiral readouts with self-navigated motion correction. Magn. Reson. Med 70, 404–412. 10.1002/mrm.24473 [PubMed: 23001771]

Johnson CL, Schwarb H, McGarry MDJ, Anderson AT, Huesmann GR, Sutton BP, Cohen NJ, 2016 Viscoelasticity of subcortical gray matter structures. Hum. Brain Mapp 37, 4221–4233. 10.1002/hbm.23314 [PubMed: 27401228]

Johnson CL, Schwarb H, Horecka KM, McGarry MDJ, Hillman CH, Kramer AF, Cohen NJ, Barbey AK, 2018 Double dissociation of structure-function relationships in memory and fluid intelligence observed with magnetic resonance elastography. Neuroimage 171, 99–106. 10.1016/j.neuroimage.2018.01.007 [PubMed: 29317306]

Kashif AS, Lotz TF, McGarry MD, Pattison AJ, Chase JG, 2013 Silicone breast phantoms for elastographic imaging evaluation. Med. Phys 40, 063503 10.1118/1.4805096 [PubMed: 23718614]

Le Y, Glaser K, Rouviere O, Ehman R, Felmlee JP, 2006 Feasibility of simultaneous temperature and tissue stiffness detection by MRE. Magn. Reson. Med 55, 700–705. 10.1002/mrm.20801 [PubMed: 16463357]

Leclerc GE, Debernard L, Foucart F, Robert L, Pelletier KM, Charleux F, Ehman R, Ho Ba Tho M, Bensamoun SF, 2012 Characterization of a hyper-viscoelastic phantom mimicking biological soft tissue using an abdominal pneumatic driver with magnetic resonance elastography (MRE). J. Biomech 45, 952–957. 10.1016/j.jbiomech.2012.01.017. [PubMed: 22284992]

Lefebvre PM, Tes Ve Koon K, Brusseau E, Nicolle S, Palieme JF, Lambert SA, Grenier D, 2016 Comparison of viscoelastic property characterization of plastisol phantoms with magnetic resonance elastography and high-frequency rheometry. Proc. Annu. Int. Conf. IEEE Eng. Med. Biol. Soc. 1216–1219. 10.1109/EMBC.2016.7590924

Manduca A, Oliphant TE, Dresner MA, Mahowald JL, Kruse SA, Amromin E, Felmlee JP, Greenleaf JF, Ehman RL, 2001 Magnetic Resonance Elastography: Non-Invasive Mapping of Tissue Elasticity. Med. Image Anal 5, 237–254. [PubMed: 11731304]

McGarry MDJ, Van Houten EEW, Johnson CL, Georgiadis JG, Sutton BP, Weaver JB, Paulsen KD, 2012 Multiresolution MR elastography using nonlinear inversion. Med. Phys 39, 6388–6396. 10.1118/1.4754649 [PubMed: 23039674]

McGarry MDJ, Van Houten EEW, 2008 Use of a Rayleigh damping model in elastography. Med. Biol. Eng. Comput 46, 759–766. 10.1007/s11517-008-0356-5 [PubMed: 18521645]

McIlvain G, Schwarb H, Cohen NJ, Telzer EH, Johnson CL, 2018 Mechanical properties of the in vivo adolescent human brain. Dev. Cogn. Neurosci 34, 27–33. 10.1016/j.dcn.2018.06.001 [PubMed: 29906788]

Murphy MC, Huston J, Glaser KJ, Manduca A, Meyer FB, Lanzino G, Morris JM, Felmlee JP, Ehman RL, 2013 Preoperative assessment of meningioma stiffness using magnetic resonance elastography. J. Neurosurg 118, 643–648. 10.3171/2012.9.JNS12519 [PubMed: 23082888]

Murphy MC, Huston J, Jack CR, Glaser KJ, Manduca A, Felmlee JP, Ehman RL, 2011 Decreased brain stiffness in Alzheimer's disease determined by magnetic resonance elastography. J. Magn. Reson. Imaging 34, 494–498. 10.1002/jmri.22707 [PubMed: 21751286]

Murphy MC, Jones DT, Jack CR, Glaser KJ, Senjem ML, Manduca A, Felmlee JP, Carter RE, Ehman RL, Huston J, 2016 Regional brain stiffness changes across the Alzheimer's disease spectrum. NeuroImage Clin. 10, 283–290. 10.1016/j.nicl.2015.12.007 [PubMed: 26900568]

Murphy MC, Manduca A, Trzasko JD, Glaser KJ, Huston J, Ehman RL, 2018 Artificial neural networks for stiffness estimation in magnetic resonance elastography. Magn. Reson. Med 80, 351–360. 10.1002/mrm.27019 [PubMed: 29193306]

Muthupillai R, Lomas DJ, Rossman PJ, Greenleaf JF, Manduca A, Ehman RL, 1995 Magnetic Resonance Elastography by Direct Visualization of Propagating Acoustic Strain Waves. Science 269, 1854–1857. [PubMed: 7569924]

Normand V, Lootens DL, Amici E, Plucknett KP, Aymard P, 2000 New insight into agarose gel mechanical properties. Biomacromolecules 1, 730–738. 10.1021/bm005583j [PubMed: 11710204]

Pattison AJ, McGarry M, Weaver JB, Paulsen KD, 2014 Spatially-resolved hydraulic conductivity estimation via poroelastic magnetic resonance elastography. IEEE Trans. Med. Imaging 33, 1373–1380. 10.1109/TMI.2014.2311456 [PubMed: 24771571]

Plewes DB, Bishop J, Samani A, Sciarretta J, 2000 Visualization and quantification of breast cancer biomechanical properties with magnetic resonance elastography. Phys. Med. Biol 45, 1591–1610. [PubMed: 10870713]

Rüther A, Forget A, Roy A, Carballo C, Mießmer F, Dukor RK, Nafie LA, Johannessen C, Shastri VP, Lüdeke S, 2017 Unravelling a Direct Role for Polysaccharide β-Strands in the Higher Order Structure of Physical Hydrogels. Angew. Chemie - Int. Ed 56, 4603–4607. 10.1002/anie.201701019

Sack I, Jöhrens K, Würfel J, Braun J, 2013 Structure-sensitive elastography: on the viscoelastic powerlaw behavior of in vivo human tissue in health and disease. Soft Matter 9, 5672–5680. 10.1039/c3sm50552a

Schmidt JL, Tweten DJ, Benegal AN, Walker CH, Portnoi TE, Okamoto RJ, Garbow JR, Bayly PV, 2016 Magnetic resonance elastography of slow and fast shear waves illuminates differences in shear and tensile moduli in anisotropic tissue. J. Biomech 49, 1042–1049. 10.1016/j.jbiomech.2016.02.018 [PubMed: 26920505]

Schwarb H, Johnson CL, Mcgarry MDJ, Cohen NJ, 2016 Medial temporal lobe viscoelasticity and relational memory performance. Neuroimage 132, 534–541. 10.1016/j.neuroimage.2016.02.059 [PubMed: 26931816]

Solamen LM, McGarry MDJ, Tan L, Weaver JB, Paulsen KD, 2018 Phantom evaluations of nonlinear inversion MR elastography. Phys. Med. Biol 63, 145021 10.1088/1361-6560/aacb08. [PubMed: 29877194]

Su Y, Chu B, Gao Y, Wu C, Zhang L, Chen P, Wang X, Tang S, 2013 Modification of agarose with carboxylation and grafting dopamine for promotion of its cell-adhesiveness. Carbohydr. Polym 92, 2245–2251. 10.1016/j.carbpol.2012.12.003 [PubMed: 23399284]

Van Houten EEW, Miga MI, Weaver JB, Kennedy FE, Paulsen KD, 2001 Three-dimensional subzone-based reconstruction algorithm for MR elastography. Magn. Reson. Med 45, 827–837. [PubMed: 11323809]

Van Houten EEW, Viviers D. vR., McGarry MDJ, Perrĩez PR, Perreard II, Weaver JB, Paulsen KD, 2011 Subzone based magnetic resonance elastography using a Rayleigh damped material model. Med. Phys 38, 1993–2004. 10.1109/EMBC.2012.6345961 [PubMed: 21626932]

Yasar TK, Royston TJ, Magin RL, 2013 Wideband MR elastography for viscoelasticity model identification. Magn. Reson. Med 70, 479–489. 10.1002/mrm.24495 [PubMed: 23001852]

Yoshida A, Kato H, Kuroda M, Hanamoto K, Yoshimura K, Shibuya K, Kawasaki S, Tsunoda M, Kanazawa S, Hiraki Y, 2004 Development of a phantom compatible for MRI and hyperthermia using carrageenan gel - Relationship between T1and T2 values and NaCl concentration. Int. J. Hyperth 20, 803–814. 10.1080/0265673042000199268

Zarrintaj P, Manouchehri S, Ahmadi Z, Saeb MR, 2018 Agarose-based biomaterials for tissue engineering. Carbohydr. Polym 187, 66–84. 10.1016/j.carbpol.2018.01.060 [PubMed: 29486846]

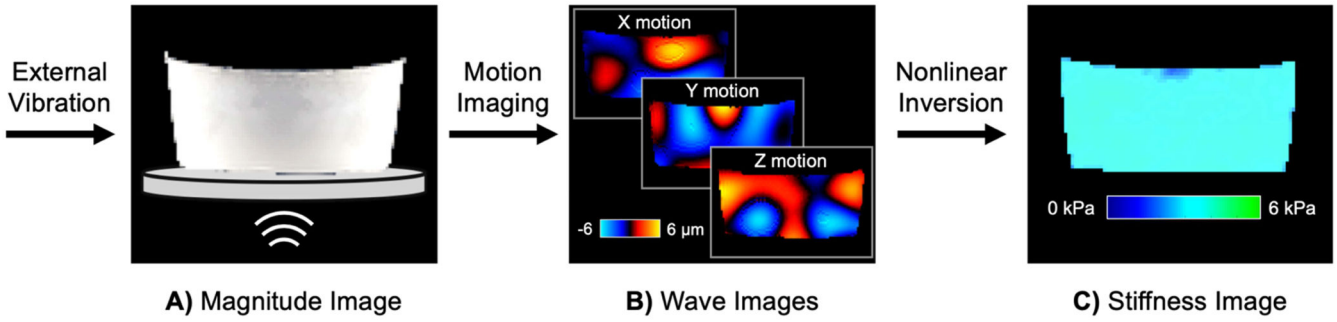

Figure 1.

Illustration of application of MRE technique on a single homogenous phantom: A) Magnitude image with pneumatic actuator paddle; B) wave propagation in x, y, and z directions; and C) shear stiffness map after nonlinear inversion

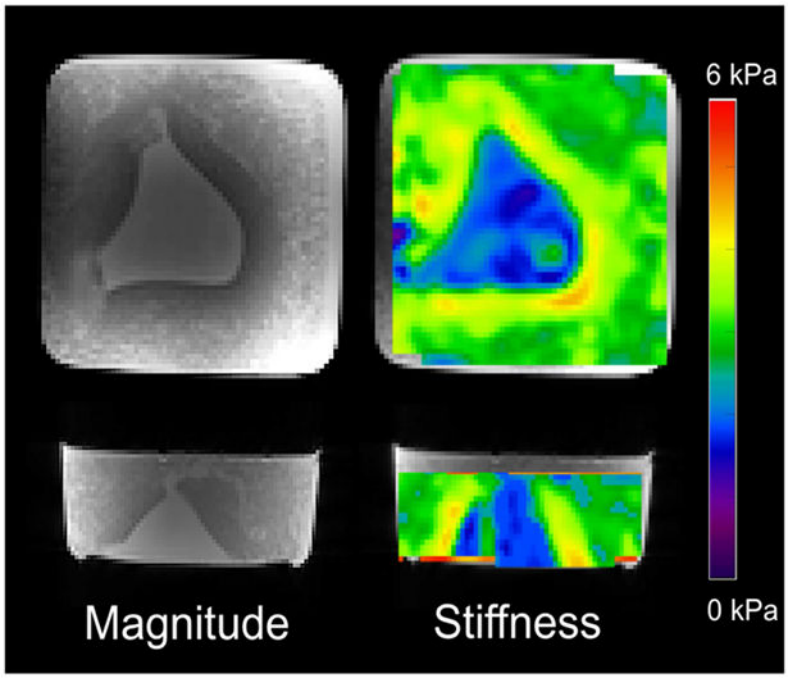

Figure 2.

Example of inhomogeneous agarose phantom demonstrating both large structural inhomogeneities in the magnitude image and stiffness map. Phantoms exhibiting such inhomogeneities were considered failures in this study.

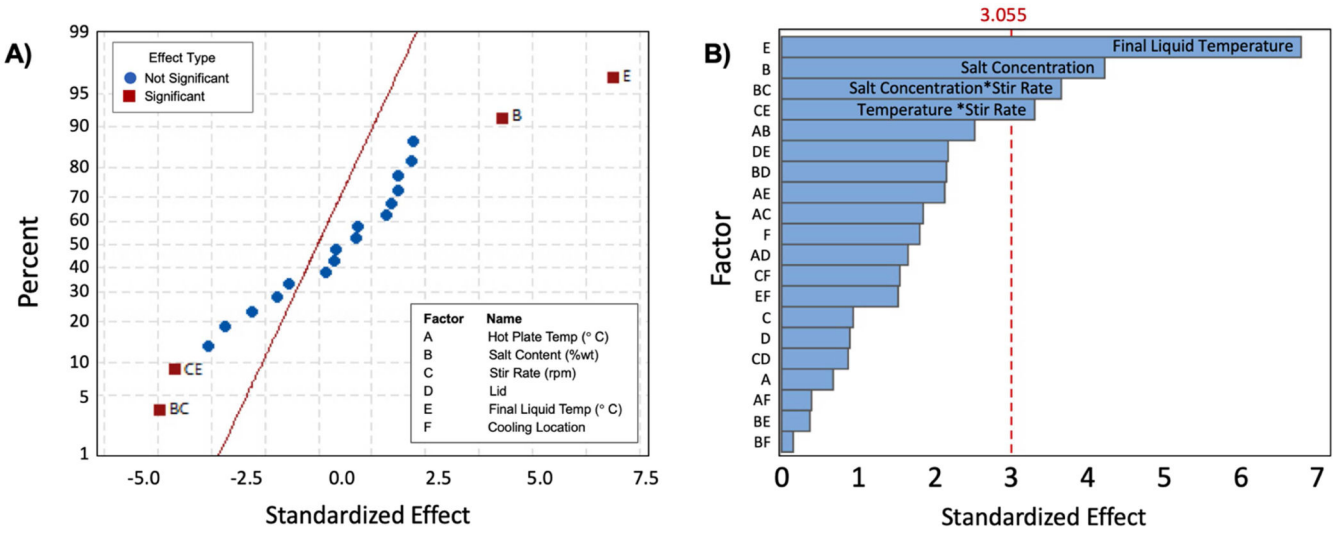

Figure 3.

A) Normal and B) pareto plots of parameter effects on stiffness, μ, at the 99% confidence level Factors B (salt content) and E (final liquid temperature), as well as the interactions BC (salt concentration and stir rate) and CE (stir rate and final liquid temperature), have statistically significant effects on stiffness.

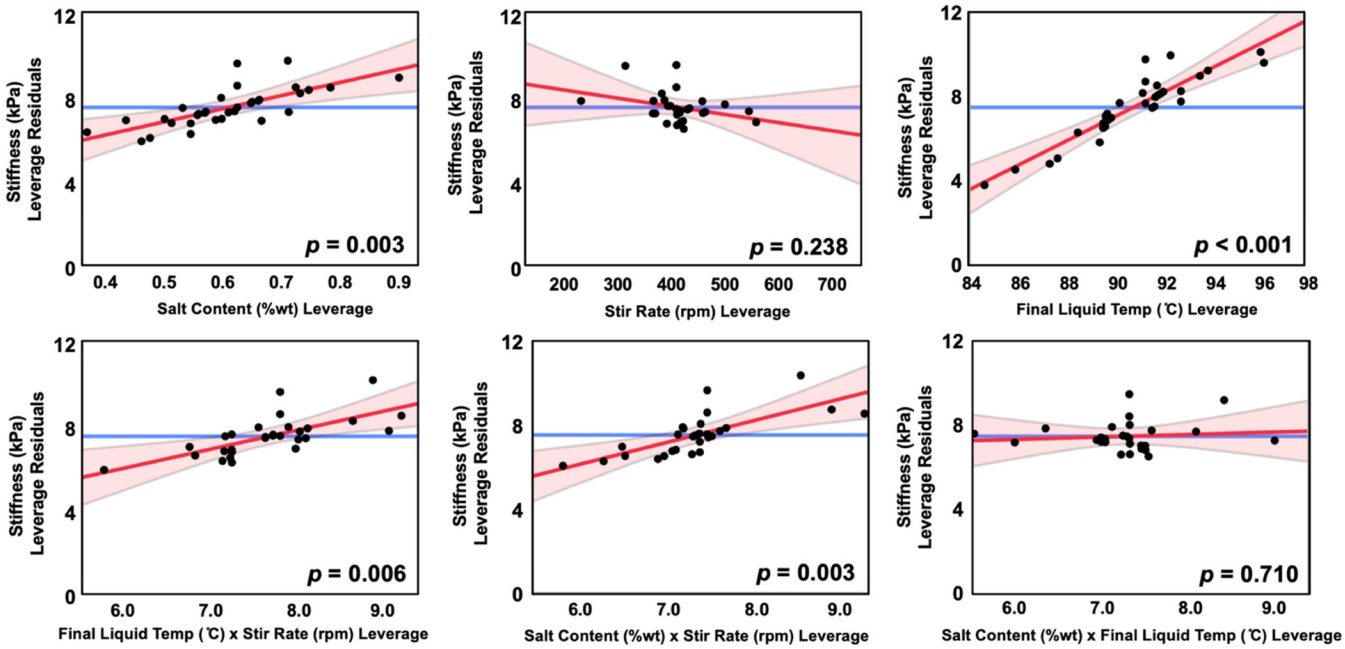

Figure 4:

Leverage residuals of factors of interest, salt content, stir rate, and final liquid temperature, as well as their interaction terms. Leverage residual plots are used to visualize the influence of data points on the model of phantom stiffness. Significant factors of interest are determined at $p < 0.01$ and are included in the model.

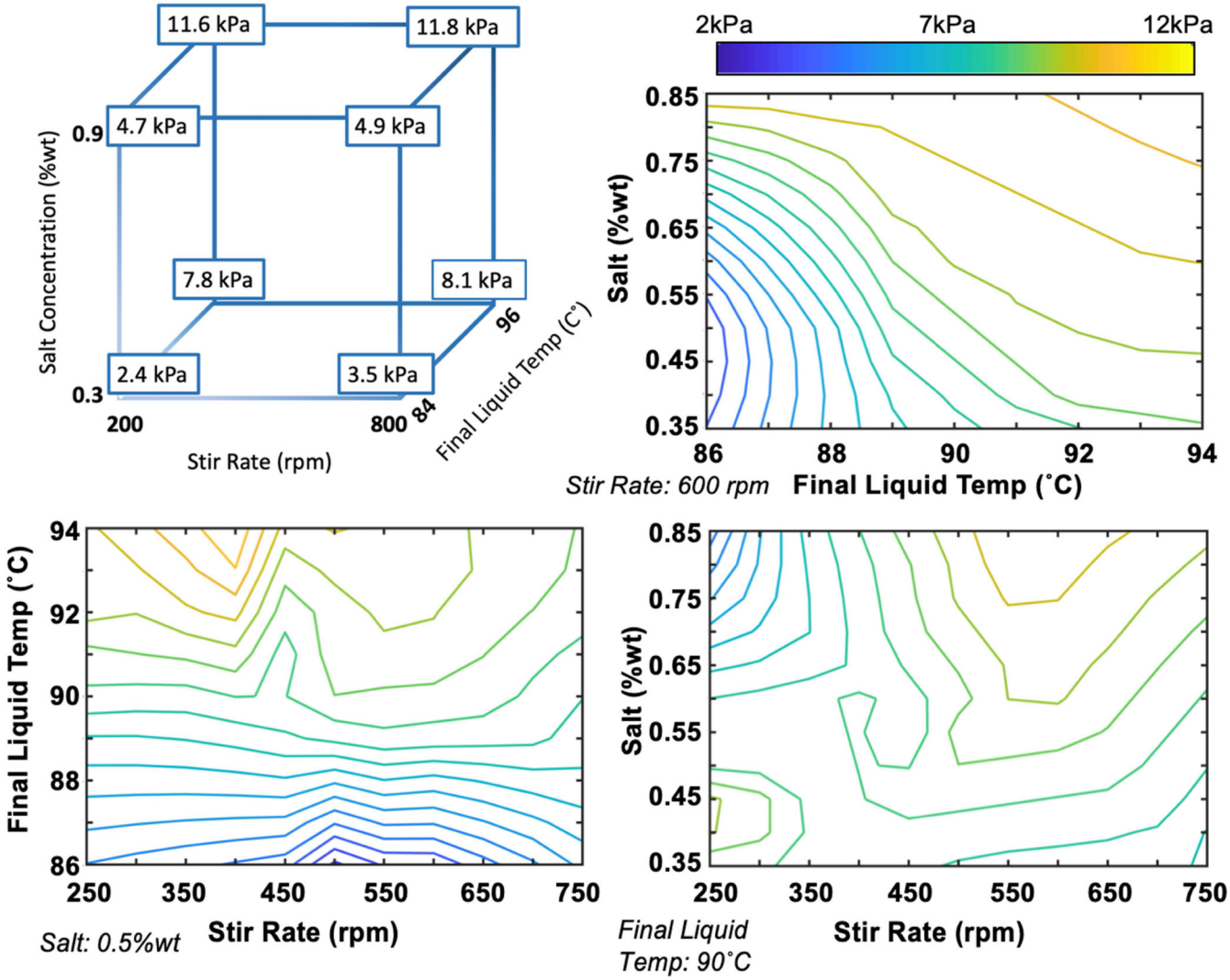

Figure 5.

Cube plot and contour plots illustrating effects of salt content, stir rate, and final liquid temperature, and their interactions on phantom stiffness.

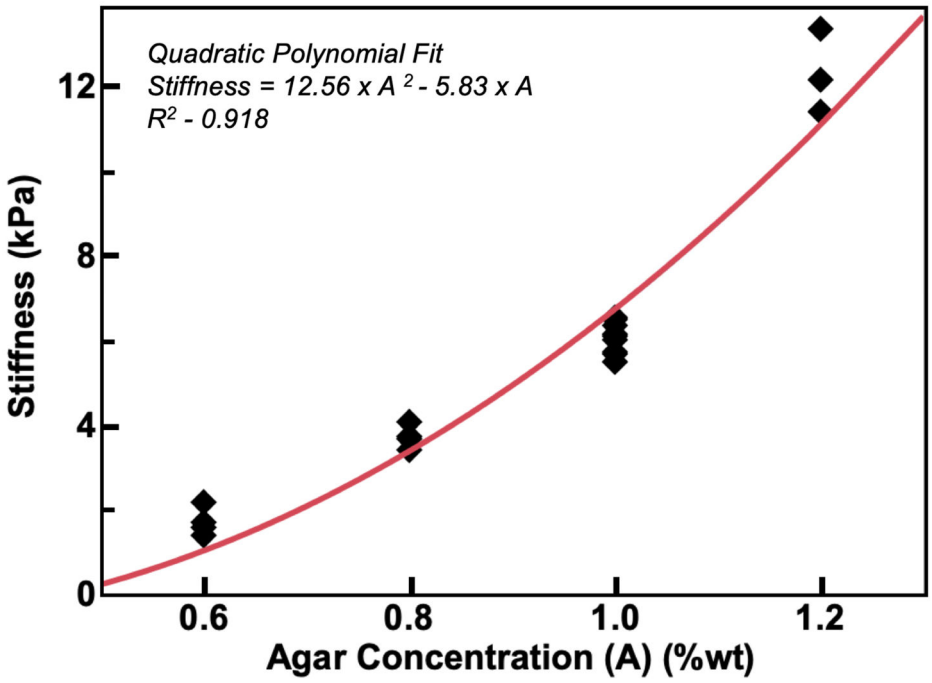

Figure 6:

Phantom stiffness dependence on agar concentration fit with a quadratic model $\mu = 12.56\ A^2 - 5.83A$ with adjusted $R^2 = 0.918$.

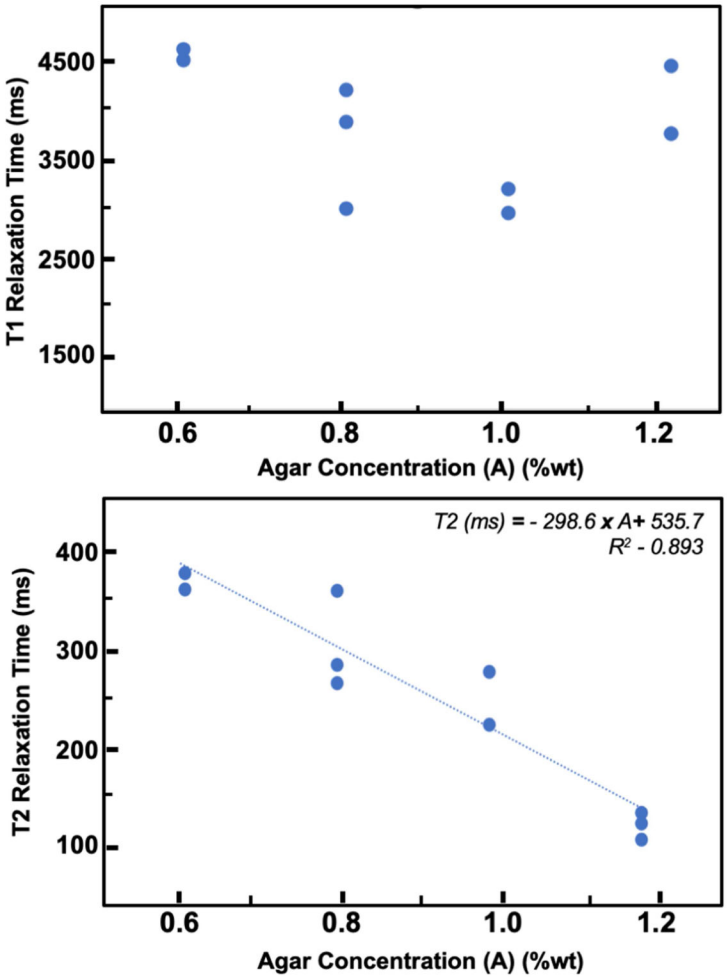

Figure 7:

T_1 and T_2-relaxation times of agarose phantoms as a function of agar concentration, A (in %wt)

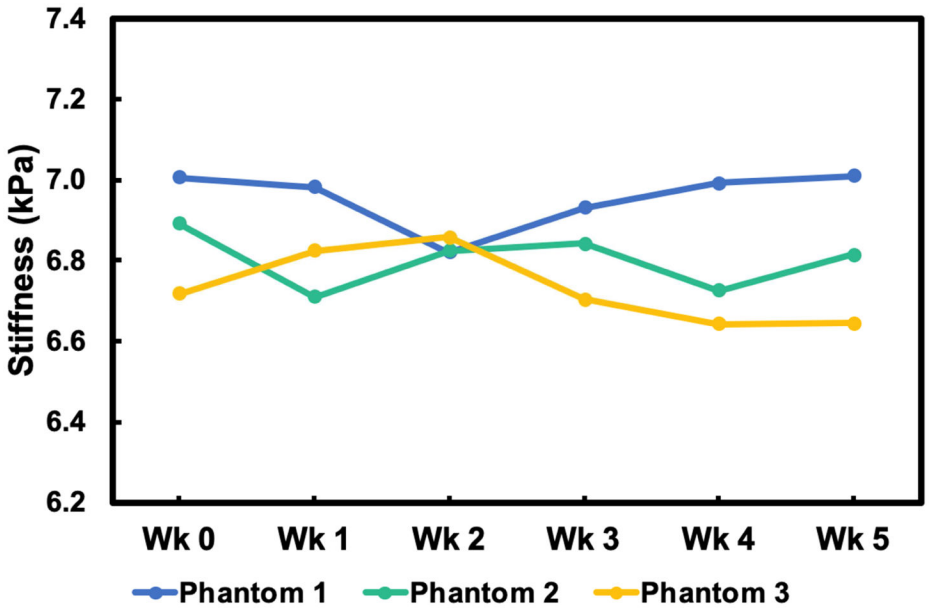

Figure 8.
Long-term stability of mechanical properties of three agarose phantoms over a five-week period

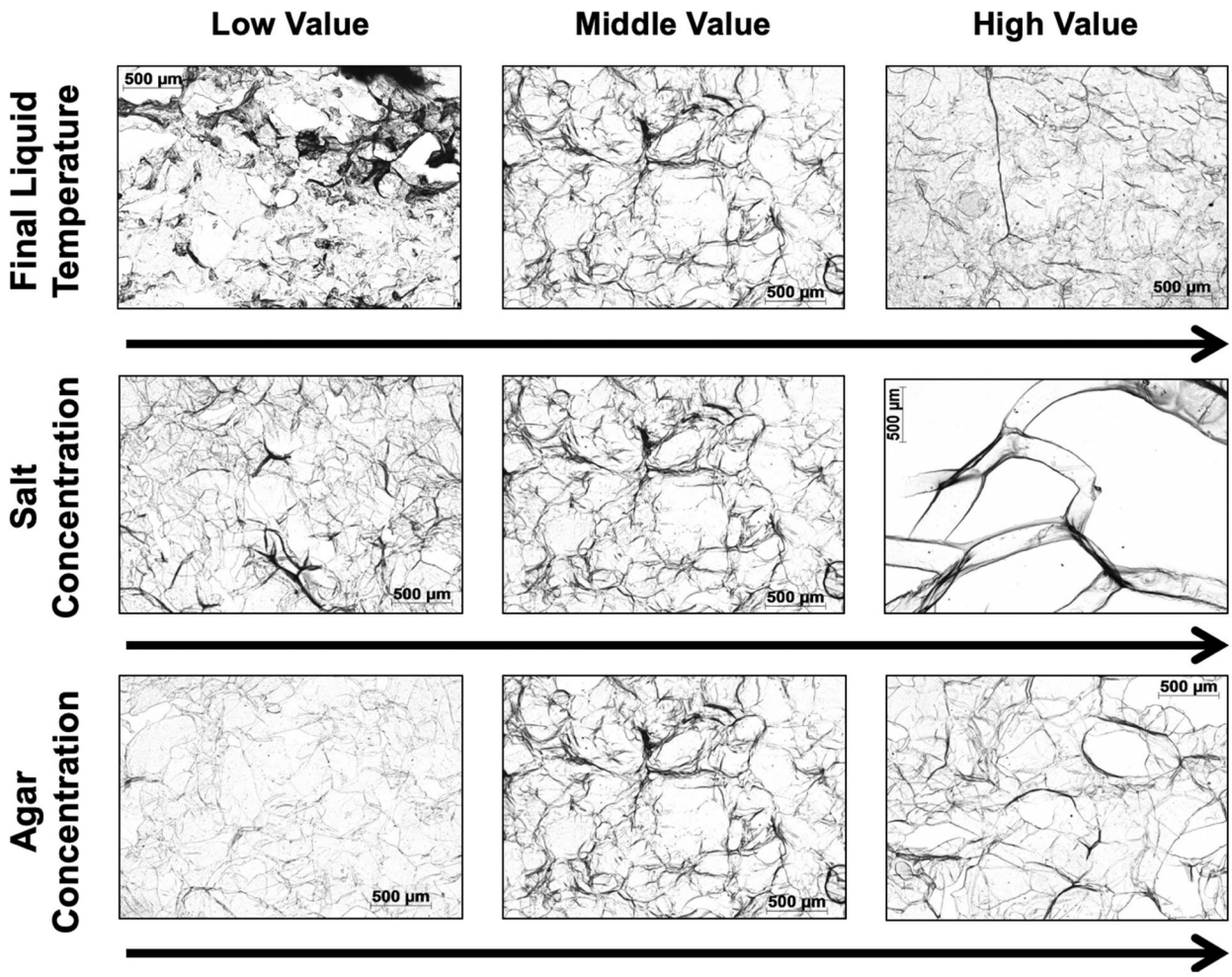

Figure 9.

Microscopy images of agar gel demonstrating microstructural changes that arise in agar phantoms with preparation protocol. Middle value images were created at 90 °C, 0.6%wt salt concentration, and 1.0% agar concentration. The other images were created by holding other parameters and varying only parameter of interest: (Top) Temperature (84, 90, 96 °C); (Middle) salt concentration (0.3%wt, 0.6%wt, 0.9%wt); and (Bottom) agar concentration (0.6%wt, 1.0%wt, 1.4%wt).

Table 1:

Effect magnitude (η^2) and associated p-values for each of the tested parameters on phantom stiffness. A resolution IV fractional factorial design was used to 19 phantoms from which parameter significance was assessed.

	Hot Plate Temperature 300 °C – 550 °C	**Salt Content 0.3%wt – 0.9%wt**	**Stir Rate 100 rpm – 800 rpm**	**Lid with or without**	**Final Liquid Temperature 84 °C- 96 °C**	**Cooling Location Ice bath, refrigerator, or room temperature**
Stiffness, μ	$\eta^2 = 0.007$ $p = 0.387$	$\eta^2 = 0.106$ $p = 0.001$	$\eta^2 < 0.001$ $p = 0.936$	$\eta^2 = 0.010$ $p = 0.296$	$\eta^2 = 0.161$ $p < 0.001$	$\eta^2 = 0.018$ $p = 0.161$

Table 2:

Mean (and standard deviation) of phantom T_1- and T_2-relaxation times at different agar concentrations across phantoms.

Agar Concentration (%wt)	T_1-Relaxation Time (s)	T_2-Relaxation Time (ms)
0.6	3.75 (0.46)	346.8 (37.3)
0.8	3.21 (0.48)	298.9 (33.4)
1.0	2.82 (0.42)	260.32 (30.3)
1.2	3.39 (0.49)	166.43 (13.5)